Numerical Simulations of Unsteady Flows Around Reentry Capsules

M. Rasquin[13], *A. Viré*[2], *Z. Djoudi*[1], *Y. Detandt*[13] *and G. Degrez*[13]
[1]*Université Libre de Bruxelles, Faculté des Sciences Appliquées*
CP165/41, avenue F. D. Roosevelt 50, B1050 Bruxelles, Belgique
[2]*Université Libre de Bruxelles, Faculté des Sciences*
CP231, Boulevard du Triomphe, B1050 Bruxelles, Belgique
[3]*von Karman Institute for Fluid Dynamics*
Chaussée de Waterloo 72, B1640 Rhode-Saint-Genèse, Belgique

Abstract

At low speed, before the splashdown, the turbulent flow field induces unsteady forces around an entry capsule. In particular, even if the capsule geometry is axisymmetric, the flow field is not axisymmetric. The understanding of these phenomena is essential to ensure both static and dynamic stability. The aim of the present study is to analyse numerically the flow field around an entry capsule at low and moderate Reynolds numbers, using a mixed spectral/finite element solver. Apollo is chosen as the representative geometry. The results obtained are compared qualitatively with experiments at low speed [1] and quantitatively with literature data at higher Reynolds numbers [2].

1. Introduction

Atmospheric entry capsules have been widely used in space missions and planetary exploration for more than 40 years. The interest for such blunt bodies has come back to the foreground recently. Indeed, in 1998, the European Space Agency (ESA) started the ARD project (Atmospheric Reentry Demonstrator) to analyse amongst other the reentry phase in the atmosphere and the opening phase of the parachutes in the final stage of the flight. Even more recently, the National Aeronautics and Space Administration (NASA) announced in 2005 its intention to flight back to the moon with a reentry capsule model. A lot of extra-planetary exploration missions have also been conducted lately, involving capsule-type geometries.

This very short introduction shows the renewed interest for the study of such flows around entry capsules. In this context, we here present a continuous work carried out at both the von Karman Institute for Fluid Dynamics and at the University of Brussels. The studied geometry is the Apollo capsule and the final stage of the flight will only be considered here, before the parachutes open so that the capsule is slowed down to a velocity of 20 km/h to reduce the impact of the splashdown.

In this work, two main parts are presented. The first part is based on experimental results and visualizations and aims at describing the main features of the flow around an entry capsule at low Reynolds numbers. Comparisons with other experimental results at higher Reynolds number are also made and the main characteristic frequencies of the flow are presented as well. The second part concerns the numerical simulations of the flow around an entry capsule at low and moderate Reynolds numbers (1000 and 10000), using an inhouse CFD code called SFELES [3, 4]. These results are then compared with the experiments we have at our disposal.

2. Description of the Flow

When a flow encounters an obstacle at a certain velocity, one can observe the development of different flow regimes, depending on the Reynolds number (*Re*). To take the example of the flow around a sphere, which is very similar to the one around a capsule, the structures downstream of the sphere can range from a stationary recirculation zone (axisymmetric flow field) at a very low *Re* (20) to a fully turbulent boundary layer with no predominant wake frequency at high *Re* ($4\ 10^5$). From $Re = 200$, the flow becomes tridimensional and for $Re \geq 800$, an unsteady wake with shear layer instabilities appears. Two main frequencies characterize these instabilities:

- a high frequency mode ($St_D = f\,U\,/\,D \simeq 2.1$) localised in the shear layer and due to a pseudo-periodic vortices release;
- a low frequency mode ($St_D \simeq 0.2$) in the remaining wake.

The knowledge of these phenomena is essential because the behaviour of the capsule can be strongly influenced by the unsteady forces induced by the flow. The experimental static and dynamic analysis of the stability around an Apollo capsule is studied extensively in [2]. The qualitative description of the flow around the Apollo capsule presented in this chapter is based on experimental results carried out in a water tunnel at the von Karman Institute for Fluid Dynamics at Re = 2000 and 3000 [1] and compared briefly with the ones from [2].

2.1 Shear layer

Contrary to a sphere, the flow separation on a capsule always occurs at the limit between the heat shield and the conic section, which induces a shear layer characterised by a pseudo-periodic vortices release at a moderate Re of a few thousands. This is illustrated in Figure 1(a). One can also observe sometimes the pairing of convected vortices downstream. In Figure 1(b), the vortices coming from the right part of the shear layer are first convected downstream of the capsule. Then, they reduce and move to the other side of the capsule before being convected far away downstream.

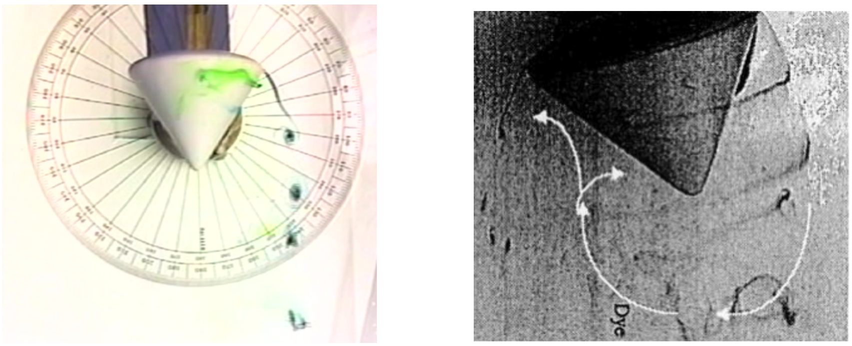

(a) Shear layer instabilities and pseudo-periodic vortices release (Re 3000).

(b) Shear layer evolution at a non zero angle of attack.

Figure 1: Shear layer instabilities.

2.2 ‘Fish tail’ motion in the wake of the capsule

The ‘fish tail’ motion in the wake of the capsule is outlined in Figure 2. The injected dye is barely convected downstream and stays in a region close to the capsule. This oscillating motion is characterized by a low frequency but a high amplitude. This fish tail motion can even interfere with the convected vortices in the shear layer, as in Figure 2.

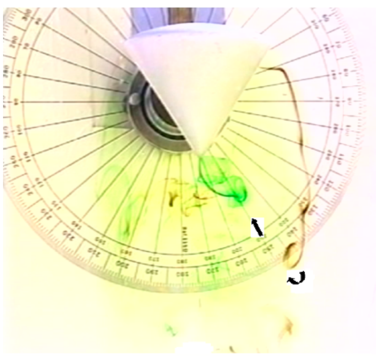

Figure 2: Shear layer instabilities and ‘fish tail’ motion (Re 3000).

2.3 Recirculation zones

Two kinds of recirculation regions can be observed close to the capsule, one characterized by a plane $\theta = cst$ and the other one developing in the azimuthal direction ($\theta \neq cst$). In a plane $\theta = cst$, one can observe that the dye is sometimes enclosed near the capsule, sometimes convected downstream. This phenomenon seems to be related to the fish tail motion described in Section 2.2. When the fish tail is moving from left to right in Figure 3(a), the flow accumulates near the wall in that region. Then, the generated recirculation zone is in a way surrounded by the fish tail motion and by the shear layer, with the possibility to spread only in the azimuthal direction (Figure 3(c)).
On the other hand, when the fish tail motion is moving from right to left (Figure 3(b)), the recirculation zone can be convected downstream by the shear layer. In the azimuthal direction (Figure 3(c)), the recirculation zones correspond to tridimensional effects.

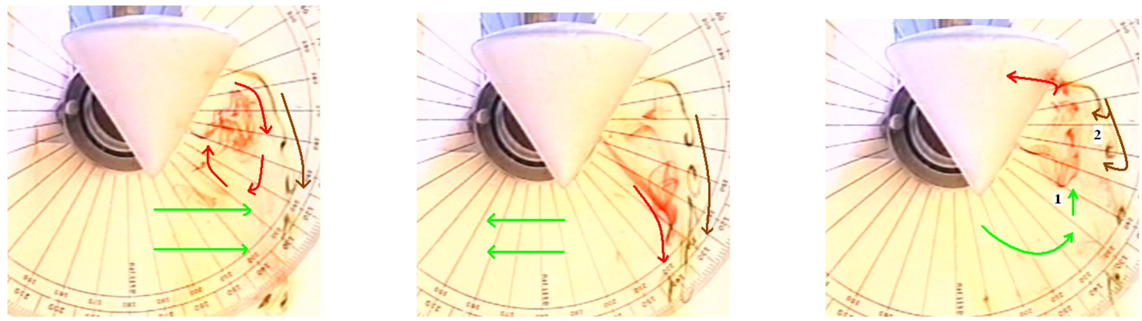

(a) Interaction between the'fish tail' motion and the recirculation zone along the capsule with the 'fish tail' motion approaching the underlined shear layer.

(b) Interaction between the'fish tail' motion and the recirculation zone along the capsule with the 'fish tail' motion moving away from the underlined shear layer.

(c) 3D effects in the azimuthal direction.

Figure 3: Recirculation zones (Re 2000).

2.4 Characteristic frequencies

The characteristic frequencies of the flow around a capsule are very similar to the ones around a sphere as described above. Experiments carried out in the work of Ö. Karatekin [2] yield $St_D \simeq 2.1$ for the formation of ring vortices. According to his work, this result is also independent from the *Re* number as well as from the angular position. In the near wake of the capsule, he found approximately a mean $St_D = 0.17$ at a zero angle of attack ($\alpha = 0^\circ$) and a mean $St_D = 0.22$ at $\alpha = 15^\circ$, independently of the *Re* number.

3. Numerical simulations

The numerical framework used for these simulations is the mixed Spectral/Finite-element Large Eddy Simulation code SFELES [3, 4], developed at the von Karman Institute for Fluid Dynamics, Brigham Young University and University of Brussels. This code allows simulation of 3D unsteady incompressible and turbulent flows around axisymmetric geometries of arbitrary complexity and offers a natural decomposition of a fully three-dimensional problem into a set of two-dimensional problems. The governing equations are discretized in planes $\theta = cst$, using linear finite-elements. The transverse azimuthal direction of the flow field is represented by means of a truncated Fourier series which assumes periodicity in the θ direction.
The flow is computed around an Apollo entry capsule whose geometry is shown in Figure 4(a). The direction of the axis for this test case is precised in Figure 4(b). Two series of computations were made at different *Re* numbers. The first one was performed at $Re = 1000$, using direct numerical simulation (DNS) which simulates all turbulent scales present in the flow. The second series was carried out at $Re = 10000$, using large eddy simulation (LES) in order to model the smallest turbulent scales. In both cases, since P1/P1 elements are used in our finite element discretization, PSPG terms are needed to stabilize the pressure oscillations. Moreover, a 4^{th} order laplacien is also coupled with the Navier-Stokes equations in order to avoid velocity oscillations during the computation at $Re = 1000$. At $Re = 10000$, a traditional SUPG stabilization is rather used.
For both *Re* numbers, 2 angles of attack (α) are considered: 0° and 15°. For the $\alpha = 0^\circ$ case, some white noise (1%) is introduced during the computation to help the axisymmetric flow to become fully $3D$. For the $\alpha = 15^\circ$ case, this

'trick' is not required since the flow is intrinsiqually not axisymmetric. Nevertheless, the solutions with and without noise are computed in order to analyze the influence of this parameter. 32 Fourier modes are also used in the azymuthal direction, with only 16 active in order to avoid the aliasing phenomenon.
The characteristic frequencies of the flow are found by means of probes arranged in either the shear layer region or in the wake of the capsule. The frequency analysis is then performed by computing the power spectrum density of the discrete temporal signal.
The forces and moments acting on the body of the capsule are also computed and some of their aerodynamic coefficients are shown below.

- Drag coefficient: $C_D = 2\,D\,/\,(\rho\,V^2\,S\,)$
- Lift coefficient: $C_L = 2\,L\,/\,(\rho\,V^2\,S\,)$
- Lateral force coefficient: $C_{F_z} = 2\,F_z\,/\,(\rho\,V^2\,S\,)$
- Pitching moment coefficient: $C_{C_z} = 2\,C_z\,/\,(\rho\,V^2\,S\,\overline{c})$

These coefficients are obtained by integration of the pressure distribution only on the body of the capsule. The aerodynamic chord $\overline{c}$ is equal to the diameter of the capsule and the reference surface S is the projection surface of the shield ($S = \pi\,D^2\,/\,4$). In order to make comparisons with [2], moments are computed at the centre of gravity of the capsule, represented in Figure 4(a) by the half filled symbol ⊕.

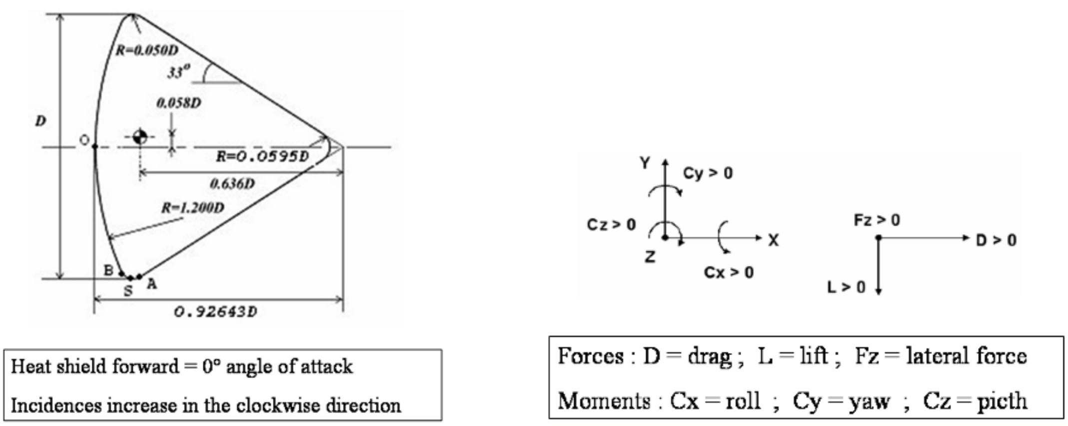

(a) Capsule geometry.

(b) Axis representation and sign convention for the aerodynamic coefficients.

Figure 4: Capsule geometry, axis representation and sign convention for the aerodynamic coefficients.

3.1 *Re* 1000

The mesh for this *Re* number contains 26000 nodes and $\Delta\,t = 5\,10^{-4}s$ is applied at each time step. The code ran first for 100 iterations. Then, the computation is restarted with or without the addition of white noise in order to activate the 3D features of the flow when needed.
First, two instantaneous representations of the flow field are presented in Figure 5. These representations outline some features of the flow already mentioned in Section 2. One can first notice that the flow is clearly not symmetric. The shear layer in the upper part of Figure 5(a) is more organized than in the lower part. Indeed, at the level of the downstream saddle point, one part of the flow coming from the upper shear layer move to the lower semi-plan, following the trajectory $1 - 2$ in Figure 5(a) before being convected downstream again. This feature was already described in Figure 1(b). Moreover, the streamlines at point 3 show the flow move upstream on both sides of the capsule head. A recirculation zone is also outlined in Figure 5(a). It is the result of the interaction between the shear layer on the first hand and the wake close to the head of the capsule on the other hand. This recirculation zone is at the origin of the flowfield in the azimuthal direction. In Figure 5(b), one part of the flow originally confined near the body of the capsule starts being convected downstream by the shear layer at the level of the junction between the shield and the conical part of the capsule. This was also observed experimentally in Figure 3(b) but a little bit more downstream, at the level of the rectangular symbol in Figure 5(b). This difference can be explained by the dye which is injected under a certain pressure in Figure 3(b) and which perturbs the flow in the wake of the capsule.

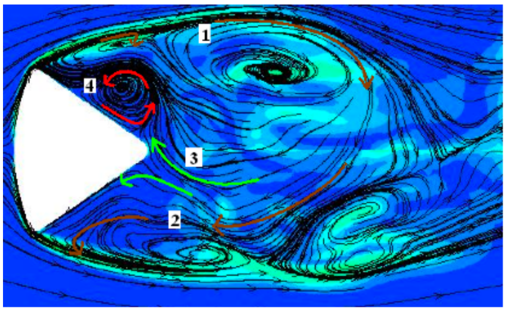

(a) Flow visualization after 60 seconds.

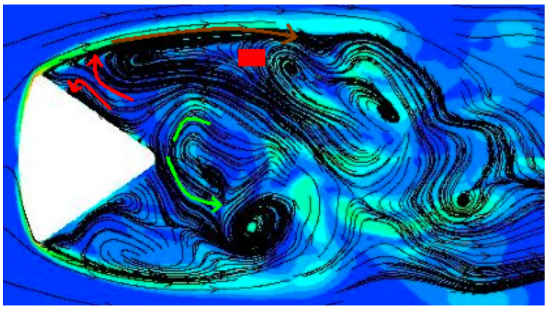

(b) Flow visualization after 50 seconds.

Figure 5: Flow visualization around the capsule at $Re = 1000$ and at 0° angle of attack, with the vorticity field as a background.

Secondly, the Fourier transform of the velocity in the azimuthal direction is applied for points located downstream of the wake. These probes manage to capture particularly well the low frequency mode of the fish tail motion and gives a mean $St_D = 0.165$ when $\alpha = 0^\circ$, which is in good agreement with the experimental data presented in Table 1.

	$\alpha = 0^\circ$			$\alpha = 15^\circ$		
	$Re = 45000$	$Re = 2.26\ 10^5$	$Re = 1.15\ 10^6$	$Re = 45000$	$Re = 2.53\ 10^5$	$Re = 1.15\ 10^6$
	[5], p.4	[2], p.222		[5], p.4	[2], p.222	
St_D	0.16	0.174	0.172	0.18 ($\alpha = 20^\circ$)	0.231	0.222

Table 1: Experimental results of St_D in the wake of the capsule for different Re at 0 and 15° angles of attack.

One example of such a spectrum is shown in Figure 6(a). For the $\alpha = 15^\circ$, some probes in the wake captures a $St_D = 0.2$, which is also in good agreement with Table 1. Unfortunately, none of the probes located in the shear layer

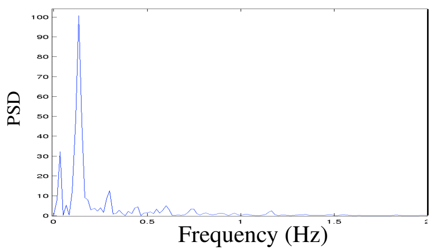

(a) Frequency spectrum of the azimuthal velocity w in a point located in the wake of the capsule at a 0° angle of attack and $Re = 1000$. Peak detected at $St_D = 0.165$.

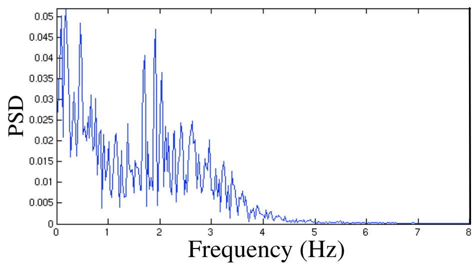

(b) Frequency spectrum of the pressure in a point located in the shear layer of the capsule at a 15° angle of attack and $Re = 10000$. Peaks detected at $St_D = 0.183$ and 1.965

Figure 6: Power spcectrum density at $Re = 1000$ and 10000.

managed to capture the high frequency mode. It is thought to be due to a too coarse mesh in the very localized shear layer region. Since all of the results are in good agreement with the experiments except the missing mode in the shear layer, no additional computation with a finer mesh were carried out at $Re = 1000$ in order to capture the high frequency mode. Nevertheless, more attention was turned to that particular point for the $Re = 10000$ case.

Thirdly, the main aerodynamic coefficients are either plotted in function of the physical time in Figures 7, 8 and 9, or presented in Table 2 with their asymptotic result. Some comparisons can then be made from experimental results summarized in Table 3.
The drag and pitching moment coefficients with $\alpha = 0^\circ$ are plotted in Figures 7(a) and 8(a) while the $\alpha = 15^\circ$ cases are represented in Figures 7(b) and 8(b) . When no noise is added during the computation with $\alpha = 0^\circ$, the flow remains purely axisymmetric and bidimensional ('$2D$ flow' in Figures 7(a) and 8(a)).

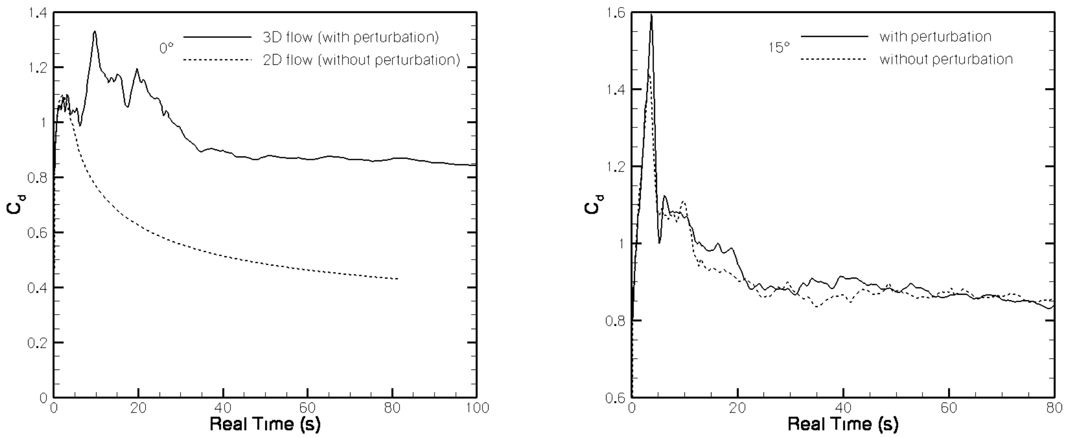

(a) $\alpha = 0^{\circ}$. (b) $\alpha = 15^{\circ}$.

Figure 7: Drag coefficients at $Re = 1000$.

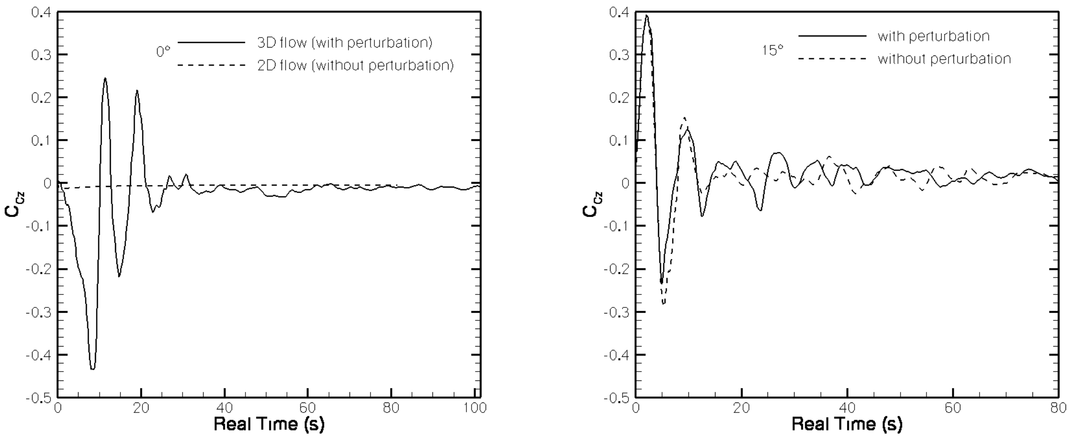

(a) $\alpha = 0^{\circ}$. (b) $\alpha = 15^{\circ}$.

Figure 8: Pitching moment coefficients at $Re = 1000$.

One can observe that the drag coefficient is much lower in the $2D$ case than in $3D$. Moreover, the $3D$ drag coefficient oscillates around a mean value of 0.85 after $80s$ of physical time while the $2D$ drag coefficient never stops decreasing. After $100s$, C_D in $2D$ is equal to 0.42. After $200s$, we find $C_D = 0.37$. So far, no data in the literature allows us to confirm this decrease or not. When $\alpha = 15^{\circ}$, no difference is observed in the behaviour of C_D whether some noise is added or not. This shows that the noise is useful to activate the $3D$ features of the flow but is not required when the flow is intrinsically not axisymmetric.
The lift coefficient C_L in Table 2 tends to 0 with $\alpha = 0^{\circ}$ as expected, even when some noise is added. Experimental results from [2] do not give $C_L = 0$ in Table 3 because the support for the experimental model is not located exactly on the symmetry axis.
When $\alpha = 0^{\circ}$, the analysis of the lateral force F_z shows that the addition of noise leads to a non zero F_z which decreases in time and tends to zero again. This is not the case any more when $\alpha = 15^{\circ}$. Indeed, one can notice in Figure 3.1 the appearance of a lateral force with a non zero angle of attack after $25s$ without any addition of noise during the computation.
The roll and yaw moment are negligible with a zero or non zero angle of attack, as Ö. Karatekin found in [2].
With regards to the pitching moment (Figure 8 and Table 2), the tridimensional effects induce a non zero C_{C_z} when

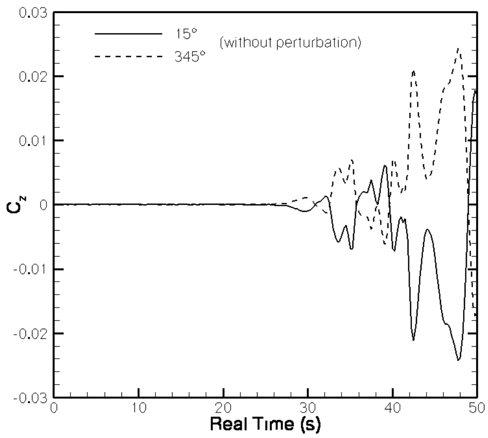

Figure 9: Lateral force coefficient at $Re = 1000$ - $\alpha = \pm 15^\circ$.

$\alpha = 0^\circ$. This can be explained by the fact that the moments are computed at the centre of gravity which is not located exactly on the symmetry axis. When $\alpha = 15^\circ$, C_{C_z} at the centre of gravity is still decreasing to zero. Indeed, the asymmetry of the centre of gravity with respect to the axis leads to an associated equilibrium position of $\alpha = 15^\circ$ and not $\alpha = 0^\circ$. This result is also confirmed by experimental data in Table 3.

	$Re = 1000$			
	$\alpha = 0^\circ$		$\alpha = 15^\circ$	
	With noise	Without noise	With noise	Without noise
C_D	0.85	0.42	-	0.83
C_L	0 ± 0.004	0	-	0.21
C_{C_z}	-0.01	-0.005	-	0.01 (still decreasing)

Table 2: Numerical results of aerodynamic coefficients at $Re = 1000$ and for 0° and 15° angles of attack.

	$Re = 60\ 10^3$		$Re = 110\ 10^3$		$Re = 200\ 10^3$		$Re = 1.2\ 10^6$	
	Experimental results [2], p.91-92				Integration of experimental C_p [2], p.91-92			
	$\alpha = 0^\circ$	$\alpha = 15^\circ$	$\alpha = 0^\circ$	$\alpha = 15^\circ$	$\alpha = 0^\circ$	$\alpha = 15^\circ$	$\alpha = 0^\circ$	$\alpha = 15^\circ$
C_D	0.985	0.93	-	-	0.966	0.95	-	-
C_L	-0.036	0.23	-	-	0.012	0.353	-	-
C_{C_z}	-	-	-0.041	0	-	-	-0.055	-0.013

Table 3: Experimental results of aerodynamic coefficients at $Re = 1000$ and for 0° and 15° angles of attack.

3.2 *Re* 10000

At this Reynolds number, the DNS computational cost would be excessive (computation cost $\sim Re^3$) and we therefore use a LES approach in which the effects of unresolved turbulent scales of the flow are modelled by means of a sub-grid scale model. In this context, the traditional Smagorinski and Wale models are used. These are the first step in the implementation of more sophisticated models and still need to be validated more intensively.
For this test case, the mesh contains 29000 nodes for $\alpha = 0^\circ$ and 35000 for $\alpha = 15^\circ$. In both cases, $\Delta t = 5\,10^{-4}s$ at each time step. Thanks to the attention turned to the mesh in the shear layer region, the high frequency mode is captured, as shown in Figure 6(b) [6]. Indeed, a peak is clearly detected at $St_D = 1.965$. This result is also confirmed by instantaneous views of the solution, not shown here. Since the proble used to plot Figure 6(b) is located a little bit

downstream of the capsule, another peak is also detected at $St_D = 0.183$ and is characteristic of the low frequency mode. The main features of the flow for this *Re* number are similar to what is already described above. With regards to the aerodynamic coefficients, the results are already in good agreement with experimental data but more time steps are still required in order to show statistics for a sufficient large time period. Let us anyway point out that a lateral force F_z is also present and does not seem to decrease, even for the $\alpha = 0^{\circ}$ case.

4. Conclusion and perspectives

The flow field analysis around a static Apollo capsule at low speed reveals the presence of two dominant quasi-periodic structures [2]. On one hand, the flow separation at the junction between the heat-shield and the conical part yields the formation of ring vortices. This shear layer instability is characterized by a Strouhal number of approximately 2.1. On the other hand, vertical oscillations ('fish tail motion' [2]), which are characterized by a low Strouhal number (approximately 0.2), are observed downstream of the wake.
Numerical simulations have been performed at Reynolds numbers of 1000 and 10000 and for incidences of 0° and 15°, the heat-shield facing the stream. Direct numerical simulation is used for the $Re = 1000$ case and large eddy simulation for $Re = 10000$. Aerodynamic coefficients are in good agreement with the literature [2] but the investigation of aerodynamic forces and moments also reveals unsteady variations due to three-dimensional effects. In particular, the study seems to support the hypothesis of F.Y. Wang [7]: oscillations of the wake closure point could be responsible of the appearance of additional swirl structures in the wake. Moreover, the simulations seem to indicate the existence of an unsteady lateral force at a 15° angle of attack. To the authors knowledge, this phenomenon had never been reported in the literature and further simulations should be conducted at different incidences in order to support this observation. In all cases, the results are independent of the Reynolds numbers, as the flow separation is determined by the geometry, which is in good agreement with [2].
Further work at higher Reynolds number is still needed to validate the already implemented turbulent models and to enrich our CFD code with more sophisticated models.
Finally, many unsteady phenomena have been observed and outlined in this study. In this context, a further numerical study about the dynamic stability of the capsule is planned as well.

Acknowledgements

A. Viré, Y. Detandt and M. Rasquin are supported by a FRIA fellowship. Developments on SFELES are supported by the Higher Education and Scientific Research Division of the French Community Government at ULB (ARC project 02/07-283). Computations are performed on the linux cluster ANIC4, financed by several contracts (http://anic4.ulb.ac.be). Experimental study has also been conducted in the von Karman Institute for Fluid Dynamics.

References

[1] A. Viré. Etude de l'écoulement autour des capsules spatiales. Master thesis, Université Libre de Bruxelles, Faculté des Sciences Appliquées, 2006.

[2] Ö. Karatekin. Aerodynamics of a planetary entry capsule at low speeds. PhD Thesis, Université Libre de Bruxelles, Faculté des Sciences Appliquées, / von Karman Institute for Fluid Dynamics, 2002.

[3] D. Snyder. A Parallel Finite-Element/Spectral LES Algorithm for Complex Two-Dimensional Geometries. PhD thesis, von Karman Institute and Utah State University, 2002

[4] Y. Detandt. Extension of a spectral/finite element code for large eddy simulations (SFELES) to axisymmetric bodies. Diploma Course Report, von Karman Institute, 2004

[5] Ö. Karatekin, F.Y. Wang and J.-M. Charbonnier. Near-wake of a three-dimensional bluff body at angles of attack. ASME Paper FEDSM98-5185, Proceedings 1998 ASME Fluids Engineering Division Summer Meeting, Washington DC, June 1998.

[6] Z. Djoudi. Simulations d'écoulements autour d'une capsule de rentrée atmosphérique. Master thesis, Université Libre de Bruxelles, Faculté des Sciences Appliquées, 2007.

[7] F.Y. Wang, Ö. Karatekin and J.-M. Charbonnier. An experimental study of the flow-field around an Apollo capsule at low speed. *AIAA 36th Aerospace Sciences Meeting and Exhibit*, Reno (NV), 1998.

This page has been purposedly left blank